Geophysical Research Letters

RESEARCH LETTER
10.1029/2020GL091651

Key Points:

- We present the first evidence for a periodic bedrock ridge (PBRs) pattern from the ExoMars 2022 landing site
- Formative paleowind directions are extrapolated from PBRs and transverse aeolian ridges
- Evidence for an Amazonian change in the wind regime are provided

Supporting Information:

- Supporting Information S1
- Figure S1
- Figure S2
- Figure S3
- Figure S4
- Figure S5
- Figure S6
- Figure S7
- Figure S8
- Figure S9
- Figure S10
- Figure S11
- Figure S12
- Table S1

Correspondence to:
S. Silvestro,
simone.silvestro@inaf.it

Citation:
Silvestro, S., Pacifici, A., Salese, F., Vaz, D. A., Neesemann, A., Tirsch, D., et al. (2021). Periodic Bedrock Ridges at the ExoMars 2022 landing site: Evidence for a changing wind regime. *Geophysical Research Letters*, *48*, e2020GL091651. https://doi.org/10.1029/2020GL091651

Received 9 NOV 2020
Accepted 23 DEC 2020

Periodic Bedrock Ridges at the ExoMars 2022 Landing Site: Evidence for a Changing Wind Regime

S. Silvestro[1,2], A. Pacifici[3], F. Salese[4,3], D.A. Vaz[5], A. Neesemann[6], D. Tirsch[7], C.I. Popa[1], M. Pajola[1], G. Franzese[1], G. Mongelluzzo[1,8], A.C. Ruggeri[1], F. Cozzolino[1], C. Porto[1], and F. Esposito[1]

[1]Istituto Nazionale di Astrofisica (INAF), Osservatorio Astronomico di Capodimonte, Napoli, Italy, [2]Carl Sagan Center, SETI Institute, Mountain View, CA, USA, [3]International Research School of Planetary Sciences, Università Gabriele D'Annunzio, Pescara, Italy, [4]Centro de Astrobiología, CSIC-INTA, Madrid, Spain, [5]Centre for Earth and Space Research of the University of Coimbra, Observatório Geofísico e Astronómico da Universidade de Coimbra, Coimbra, Portugal, [6]Freie Universität, Berlin, Germany, [7]German Aerospace Center (DLR), Institute of Planetary Research, Berlin, Germany, [8]Department of Industrial Engineering, Università di Napoli "Federico II", Napoli, Italy

Abstract Wind-formed features are abundant in Oxia Planum (Mars), the landing site of the 2022 ExoMars mission, which shows geological evidence for a past wet environment. Studies of aeolian bedforms at the landing site were focused on assessing the risk for rover trafficability, however their potential in recording climatic fluctuations has not been explored. Here we show that the landing site experienced multiple climatic changes in the Amazonian, which are recorded by an intriguing set of ridges that we interpret as Periodic Bedrock Ridges (PBRs). Clues for a PBR origin result from ridge regularity, defect terminations, and the presence of preserved megaripples detaching from the PBRs. PBR orientation differs from superimposed transverse aeolian ridges pointing toward a major change in wind regime. Our results provide constrains on PBR formation mechanisms and offer indications on paleo winds that will be crucial for understanding the landing site geology.

Plain Language Summary Oxia Planum on Mars is the landing site for the ExoMars 2022 mission. The region likely hosted a standing body of water, but the effect of the wind was also important in shaping the landscape. In this study, we first describe a set of linear ridges that, in our interpretation, were sculpted by the wind in a more recent past. We also show that the wind that formed the ridges (Periodic Bedrock Ridges) was blowing from a different direction than the ones that formed younger ripples on top, suggesting a complex geological history of wind erosion and deposition that will be further investigated during the ExoMars mission.

1. Study Area and Methods

The ESA/ROSCOSMOS ExoMars 2022 mission consists of a rover named "Rosalind Franklin" and a surface platform named "Kazachok" (J. Vago et al., 2015). In 2023, the mission will land in Oxia Planum (18.2° N; 24.3° W) to search for signs of past or present life on Mars and to perform long-term atmospheric investigations (Rodionov et al., 2017; J. L. Vago et al., 2017). Oxia Planum shows large outcrops of Noachian-aged phyllosilicates (a light-toned sedimentary/clay bearing unit) and a fan delta enriched in hydrated silicates, which record two distinct alteration environments and events (Carter et al., 2016; Lakdawalla, 2019; Pajola et al., 2017; Quantin-Nataf et al., 2016, 2021; J. L. Vago et al., 2017). The clay bearing unit is unconformably overlain by a Amazonian dark resistant unit (Adru or Capping Unit; Quantin-Nataf et al., 2016, 2021; J. L. Vago et al., 2017), which was interpreted to be remnants of an Early Amazonian (2.6 Ga) volcanic material suggesting an intense and prolonged erosion by wind (Carter et al., 2016; Pajola et al., 2017; Quantin-Nataf et al., 2016, 2021). Aeolian bedforms, such as megaripples or transverse aeolian ridges (TARs; Balme et al., 2008; Foroutan & Zimbelman, 2016; Hugenholtz et al., 2017; Zimbelman, 2010), are also widespread, testifying the key role played by the wind in shaping the surface of Oxia Planum (Balme et al., 2017; Bhardwaj et al., 2019; Ivanov et al., 2020; Pajola et al., 2017; J. L. Vago et al., 2017). Previous works about bedforms such as TARs in the landing site were limited to the rover trafficability analysis and their risk assessment estimate (Balme et al., 2017; Bhardwaj et al., 2019). Nevertheless, TARs and megaripples are crucial in recording climatic signatures on Mars and they can

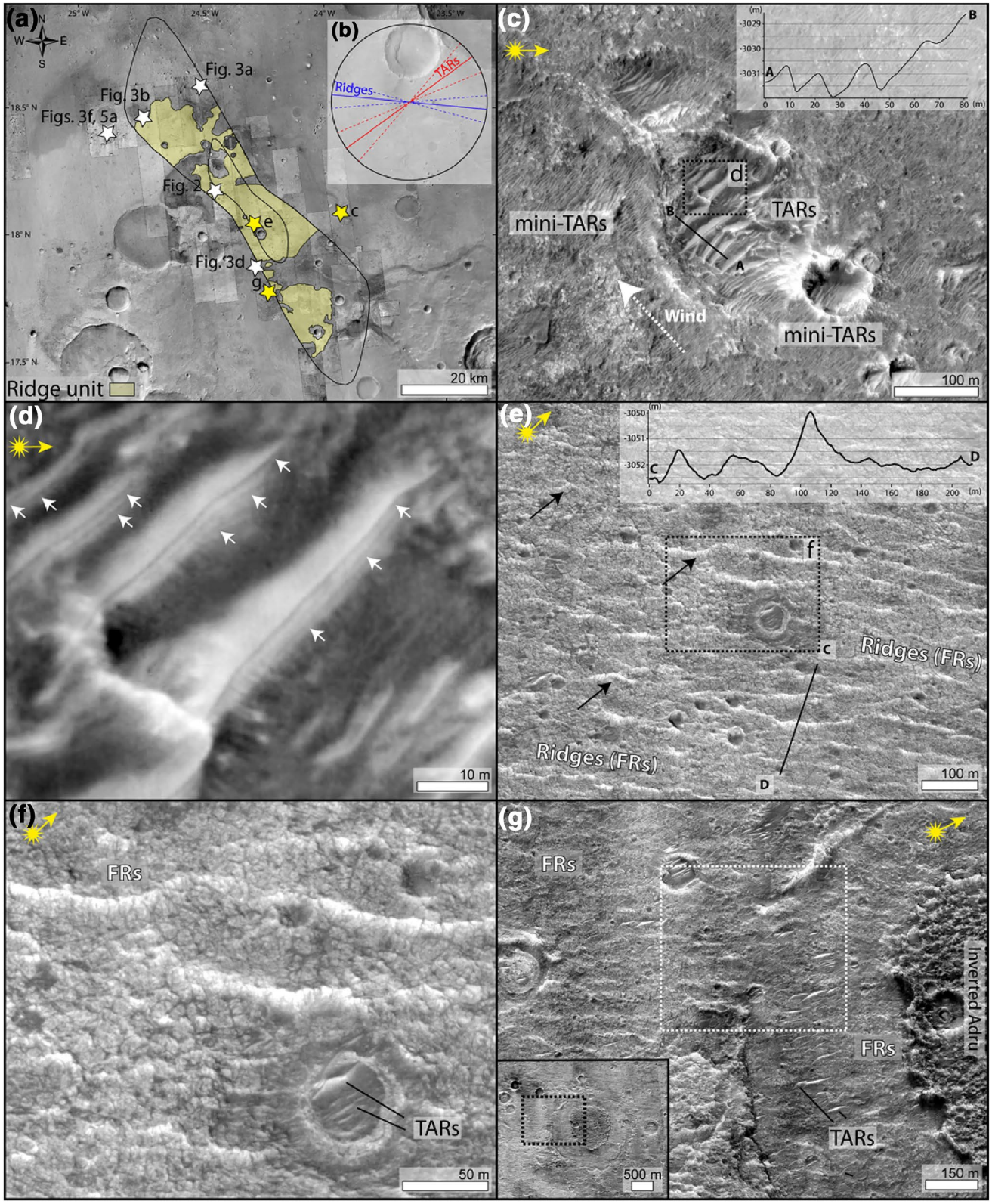
(a)
Fig. 3a
Fig. 3b
Figs. 3f, 5a
Fig. 2
Fig. 3d
c
e
g
Ridge unit
20 km
(b)
Ridges
TARs
(c)
mini-TARs
d
TARs
B
A
Wind
mini-TARs
100 m
(d)
10 m
(e)
f
c
Ridges (FRs)
Ridges (FRs)
D
100 m
(f)
FRs
TARs
50 m
(g)
FRs
FRs
TARs
500 m
150 m
Inverted Adru

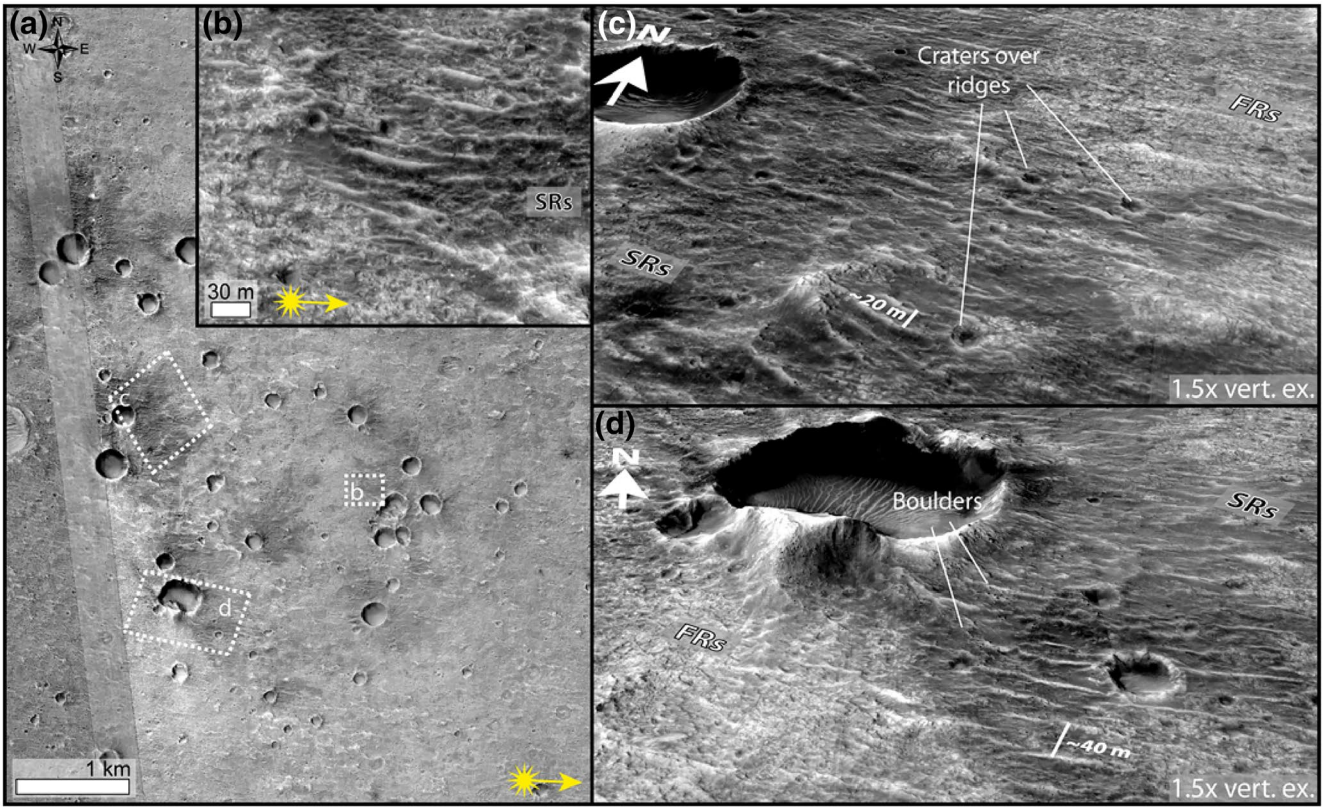

Figure 2. (a) HiRISE image showing the different albedo of the fractured ridges and smooth ridges. (b) Close-up showing details of the SRs. (c)–(d) HiRISE perspective views of the FR/SR transition. Note the same orientations and the superposition of boulders from the nearby impacts. HiRISE, High Resolution Imaging Science Experiments; FR, fractured ridge; SR, smooth ridges.

provide invaluable information on the geological history of the landing site (Day & Dorn, 2019; Fenton et al., 2015; 2018; Golombek et al., 2010; Silvestro et al., 2015; Sullivan et al., 2005). In this study, we investigate the relationship between TARs and an enigmatic EW-oriented ridge pattern that is pervasive across the ExoMars landing area (Figure 1a). We test the hypothesis of an aeolian origin for these ridges and discuss the related climatic implications.

This analysis has been made on the basis of images from the High Resolution Imaging Science Experiments (HiRISE), with a spatial resolution of 25–50 centimeter/pixel, co-registered over a 5 meters/pixel Context Camera mosaic (Dickinson et al., 2018; Malin et al., 2007; McEwen et al., 2007). Images were analyzed in ESRI's ArcGIS where TAR and ridge crestlines were mapped (Figures S1–S4) and their orientations were plotted using R statistical computing software (Figure 1b). Topographic data are derived from HiRISE Digital Terrain Models (DTMs) with a spatial resolution of 1 meter/pixel (Supplementary Table 1). The DTM (1 meter/pixel) used for deriving the profile EF (Figure 3f) was derived by using the NASA Ames Stereo Pipeline from HiRISE orbits ESP_036780_1985 and ESP_042622_1985 (Beyer et al., 2018).

Figure 1. (a) Ridge unit occurrence (mapped in yellow) at the ExoMars 2022 landing area contained within the three and one sigma envelopes of the landing ellipses. (b) Circular plot showing the average trend and circular standard deviation intervals of the mapped ridges and TARs. (c) HiRISE image showing examples of TARs and mini-TARs in the study area. Topographic profile AB derived from a HiRISE DTM (Table S1). (d) Close-up of TARs showing the exposed cross beds over the TAR stoss side (white arrows). (e) HiRISE image showing details of the fractured ridges. Black arrows point to defect terminations (Y junctions). Topographic profile CD (inset on the top right) derived from HiRISE DTM (Table S1). (f) Close-up of the FR Y junction (g) HiRISE image showing the mutual stratigraphic relationship between large eroded impacts, FRs and dark resistant unit (Adru). Note the continuity of the FR crestlines inside and outside the crater rim (white dashed box). TARs, transverse aeolian ridges; FRs, fractured ridges; HiRISE DTM, High Resolution Imaging Science Experiments Digital Terrain Models.

2. Results

2.1. TARs

The landing area is covered by aeolian bedforms which are normally referred to as TARs or megaripples (Figures 1b–d, S4 and S5; Balme et al., 2008, 2017; Berman et al., 2018; Bhardwaj et al., 2019; Foroutan & Zimbelman, 2016; Foroutan et al., 2018; Hugenholtz et al., 2017; Zimbelman, 2010). Two types of TARs have been previously detected in the landing site: regular TARs (up to a few meters in height) within impact craters and other topographic depressions and 15–25cm-tall mini-TARs found on the surrounding plains (Balme et al., 2017; Figure S4). TARs and mini-TARs are inactive bedforms (Bridges et al., 2012) as suggested by the presence of superimposed craters (Figure S5b) and locally found as continuous fields of bedforms, suggesting they belong to the same population and were formed under similar wind conditions (Figure 1c). The general trend of these bedforms in Oxia Planum, derived by mapping of 1370 TARs/mini-TARs crestlines in sampling areas, is NE-SW (53.9 ± 13.2°; Figures 1b, S4, and S5). Because TARs are thought to orient transverse to the formative wind, such a NE-SW trend can indicate winds coming from the SE or the NW. Topographic profiles of several TARs, however (Figure 1c inset), show a clear stoss and lee topography with steeper NW-dipping slopes. In addition, a set of dark and bright alternating bands following the TARs topography are locally visible over the southeastern TAR slopes (Figures 1d and S5). We interpret these layers as exposed cross beds over the erosional stoss side (see Figure S6 for clarification; Arvidson et al., 2011; Geissler, 2014; Golombek et al., 2010) indicating formative wind direction from the SE (Figure 1c). TARs and mini-TARs overlie a set of cratered ridges that cover 44% of the presumed landing area (~633 km^2; Figures 1a and 1b, 1e–1g and S7).

2.2. Ridges

Ridges are on average 38-m spaced, trend ~EW (95.4 ± 10°) and are 0.5–1.5m tall with a symmetric profile (Figure 1b, 1e, S3 and S7). Ridges display Y-junction terminations and can be visible over units with different albedo (Figures 1e–1g, 2 and S8). Based on their slope textures we recognize two ridge classes: fractured ridges (FRs) and smooth ridges (SRs) (Figures 1e–g, 2 and 3).

2.2.1. FRs

Most of the ridges in the region of study belong to this category. FRs are bright-toned, show cross-cutting fractures, and share the same blocky texture of the bedrock they are associated with (Figures 1e and 1f). Thus, FRs are lithified and directly carved into the bedrock. FR crestlines are locally found in continuity outside and inside heavily eroded impact craters (Figure 1g white dotted square) around the dark upstanding material exposed in the center (Figure 1g). Note also that the ridge crestlines on the crater floor seem slightly deflected by the dark material, suggesting the topography played an important role in controlling the formation of the ridges (Day et al., 2016). The dark material is the volcanic dark resistant unit (Adru; Quantin-Nataf et al., 2021) emplaced at the crater floor followed by rim degradation and outcropping as the inverted, flat-topped morphology visible nowadays. Similar ridge-crater relationships are visible in other areas in the study site (Figure S9). Thus, the ridge unit postdates the deposition of the Adru and the following erosional event.

2.2.2. SRs

SRs have smooth slope surfaces (not cross-cut by fractures), resembling classic TARs or megaripples (Figures 2 and 3). SRs are visible in association with impact crater ejecta and inside craters (Figures 2 and 3). SRs have similar orientation and spacing than FRs (Figure 2) and are superimposed by small (10–25 m) secondary craters and boulders, so SRs predate these impact events (Figures 2b–2d and 3). To better understand the relative age of the SRs, we mapped their occurrence on 316 craters in the study area that we qualitatively classified as relatively degraded/old and pristine/young on the basis of their state of degradation (Figures 3a, 3b and S10). Results show that SRs are only found in degraded/old craters but are never found inside pristine/young craters (Figures 3a and 3b). Thus, the SR forming process was only active in between the formation of degraded/old and pristine/young craters.

SR locally show two different crests that are faintly recognizable on HiRISE DTM (Figures 3d–3f). Both crests are truncated by craters 10–25 m in diameter, which suggest that the double crest arrangement was emplaced before the impacts (Figures 3d and 3e).

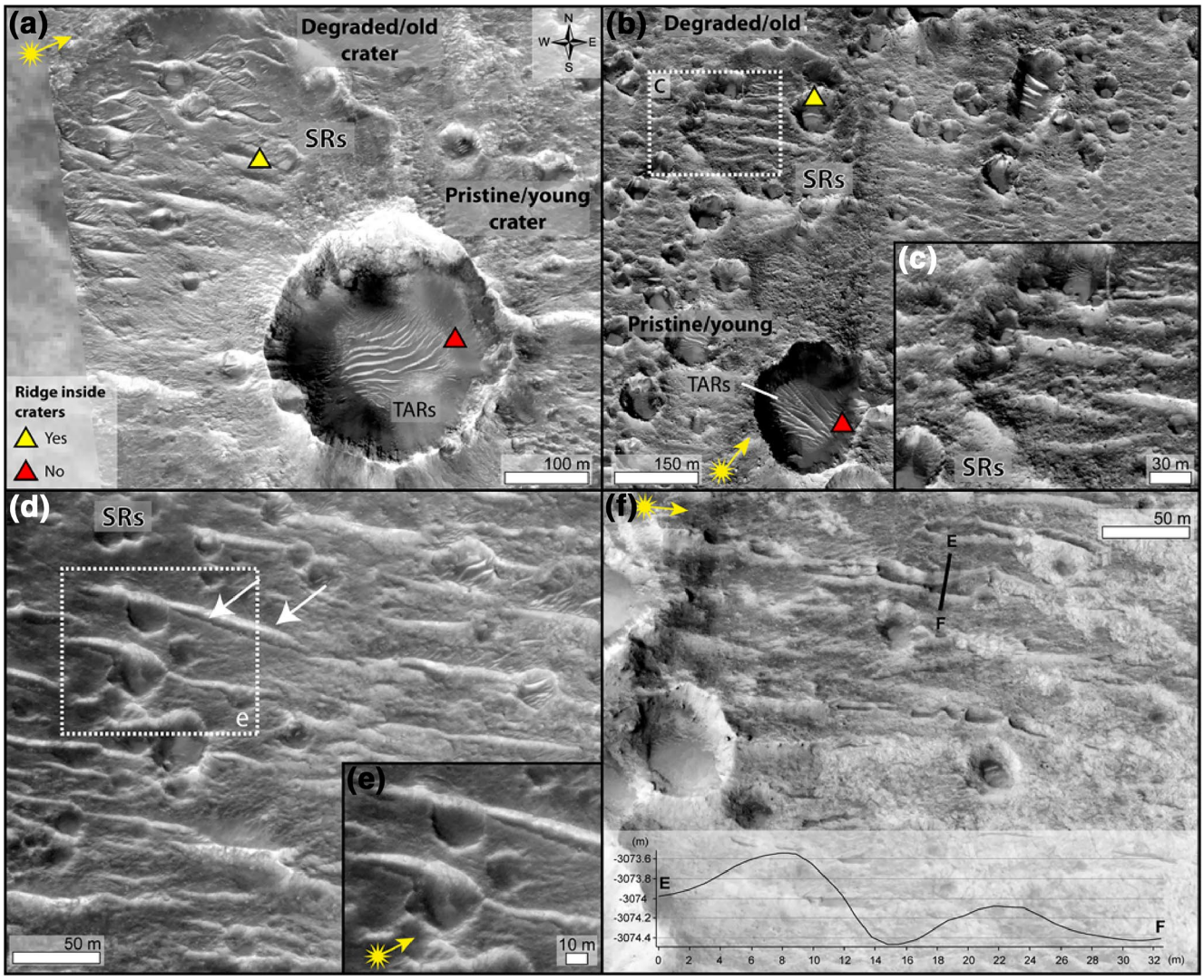

Figure 3. HiRISE image showing details of the smooth ridges . ((a)–(b)) SRs are only found in eroded/old craters and never in pristine/young ones which can be filled by TARs. Note the cratered appearance of the SRs and the stratigraphic relationship with the NE-SW oriented TARs/mini-TARs. (c) Close-up of intracrater SRs overlaid by boulders from nearby younger impacts. ((d)–(e)) SRs crossing the impact ejecta blankets showing two crests (arrowed) cut by impacts. See Figures. 1 and S8 for location. (f) Double crest structures can be locally detectable on HiRISE DTM (Profile EF). TARs, transverse aeolian ridges; HiRISE, High Resolution Imaging Science Experiments; SR, smooth ridges.

3. Discussion

3.1. An Aeolian (PBR) Origin for the Ridges

The overall regularity of the ridge crestlines seems to point toward an aeolian origin for the ridges. The fact that the ridges are mostly carved into the bedrock narrows down the possible formation process to aeolian erosion. Candidate resulting landforms are either yardangs, which are streamlined hills eroded by wind or periodic bedrock ridges (PBRs), which are bedform-like erosional features (Goudie, 2007; Hugenholtz et al., 2015; Laity, 2009; Montgomery et al., 2012). The crestlines of the ridges are not streamlined, have Y junction terminations (typical in aeolian bedforms [McKee, 1979; Werner & Kocurek, 1999]), and do not resemble yardangs at any of their formational stages (Wang et al., 2018). Their overall morphology and wavelength are rather consistent with PBRs (Montgomery et al., 2012). PBRs were hypothesized to form from the direct sand abrasion of the surface bedrock (Montgomery et al., 2012) or by bedrock erosion seeded by megaripples (Hugenholtz et al., 2015). In the latter hypothesis, the erosion of the underlying bedrock starts in ripple troughs where the substrate is exposed

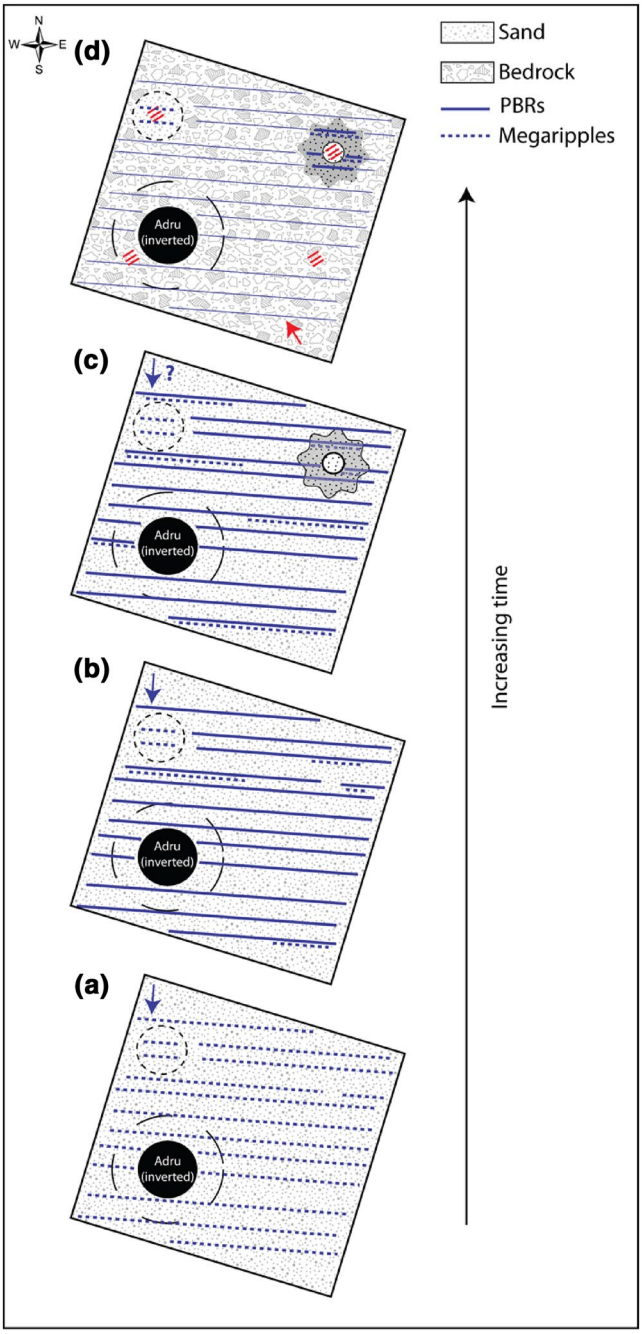

Figure 4. Schematic drawing showing the interpreted evolution of the megaripple-PBR system. (a) Deposition of the megaripples (dotted lines) in the Amazonian. (b) Formation of the PBRs (solid lines): megaripples overlie the PBRs or are locally detached. (c) New impacts strike the surface covering the megaripple/PBR pattern. (d) Erosional event: megaripples are eroded, but locally preserved were covered/sheltered. Subsequent winds deposit TARs/mini-TARs (red lines). PBRs, Periodic Bedrock Ridges; TARs, transverse aeolian ridges.

(see Figures 10a and 10b in Hugenholtz et al., 2015). Bedrock erosion continues at the pace of megaripple migration until an equilibrium is maintained between the erosion of the substrate and the bedform migration rate (Hugenholtz et al., 2015).

The estimated Amazonian age for the studied ridges (they are younger than the Adru, which was dated to Early Amazonian by Quantin-Nataf et al. (2021)), permits us to discard the hypothesis that the ridges were dune/ripples cemented by percolating water, as previously suggested for other areas on Mars (Grotzinger et al., 2005; Milliken et al., 2014). Instead, we favor the aeolian PBR origin sketched in Figure 4. A field of aeolian megaripples was deposited after the event(s) that eroded the crater rim of Figures 1g and S9a (Figure 4a). The erosional event(s) would have probably provided the necessary sand required for the formation of ~EW megaripples. Sometime, after the megaripples were deposited, incipient PBRs formed into the underlying bedrock on the plain (Figure 4b). When subsequent impacts struck the surface, the megaripple/PBR system was likely at different stages of evolution with some megaripples located on top and others downwind the PBRs (Figure 4c). Thus, the double crest arrangement shown in Figures 3d–3f can be interpreted as megaripples detaching from PBRs in agreement with the model proposed by Hugenholtz et al. (2015). Besides reinforcing the PBR hypothesis, the observation of the double crests gives also clues on the direction of the wind that formed the megaripple-PBR system: that is, it should have blown from N-NNE because the megaripples are located at the downwind side of PRBs (Figures 4 and 5). The ejecta deposited over the megaripple-PBRs favored the preservation of the megaripple crests from a subsequent episode/s of erosion that lead to the complete exposure of the PBRs on the plain (Figure 4d). In addition, the sheltering effect of the crater topography, may explain the different slope textures of the intracrater SRs that were protected from erosion and thus maintained smoother sand-covered (maybe dust-coated) surfaces (Figure 4d). In this view, SRs are the preserved megaripples that seeded the PBRs while FRs are the exposed PBRs. The wind that exposed the PBRs should not necessarily be the same that carved them or the subsequent flow that formed the TARs/miniTARs.

In an alternative scenario, SRs might represent a separate aeolian depositional event postdating the formation of the PBRs. Our observations suggest this alternative view to be less likely as the similar orientation and spacing for FRs and SRs would then be a coincidence. However, besides the interpretation of the formative flows (PBR winds will have a 180° directional ambiguity) this view will not change the main implication of this work: a main change in the wind regime followed the erosion of the PBRs in the Amazonian.

To summarize, we favor the hypothesis in which the FRs and SRs represent the same PBR-megaripple system preserved at different degrees of evolution. A major change in the wind regime occurred during or after the event that exposed the PBRs, with the winds coming from the SE becoming dominant and leading to the deposition of the TARs/mini-TARs population above the PBR/megaripples and forming the complex pattern (Kocurek & Ewing, 2005) still visible today (Figure 4d). PBRs did not form over the volcanic dark resistant unit as this is locally elevated and more resistant to erosion (Figure S11; Quantin-Nataf et al., 2016, 2019, 2021).

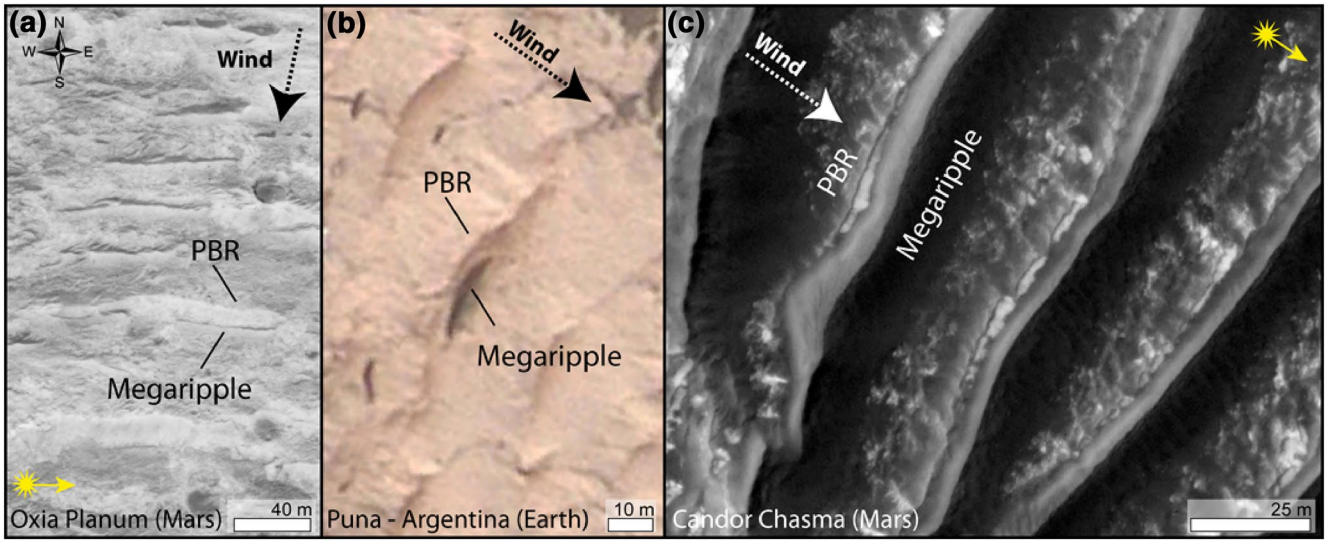

Figure 5. PBR-megaripple systems on (a) Mars, HiRISE image showing megaripples detaching from PBRs in the study area (see Figure 1a for location) and (b) Earth, Puna (Argentina; cf., Hugenholtz et al., 2015). Dark-toned megaripples are found downwind of bright PBRs (image from Google Earth). (c) HiRISE image of a similar PBR-megaripple arrangement in Candor Chasma (Mars). PBRs, Periodic Bedrock Ridges; HiRISE, High Resolution Imaging Science Experiments.

3.2. Potential Causes for a Main Wind Change

This work unveils a complex history of aeolian erosion and deposition in Oxia Planum during the Amazonian. The studied ridges and the NE-SW oriented TARs/miniTARs are relict features that recorded different wind regimes. Amazonian changes in the wind regime were hypothesized to explain the different orientation of bedforms in Meridiani Planum, the NASA Opportunity Rover landing site (Fenton et al., 2015; Golombek et al., 2010). Interestingly, a set of megaripples oriented similarly to the Oxia Planum TARs/mini-TARs were reported and attributed to an enhancing of the Hadley return-flow triggered by a decrease in the planet axial obliquity from its last relative maximum in the Late Amazonian 86–72ka (Fenton et al., 2018). Because the Hadley circulation dictates the wind regime at these latitudes (Fenton et al., 2013), we cannot exclude that the same event promoted the formation of the TARs/mini-TARs in the study area.

3.3. Implication for the ExoMars Mission

Roving in Oxia Planum will be a unique opportunity to dig inside the aeolian origin of the ridge unit, providing clues on the nature and formation mechanism of similar features observed elsewhere on Mars (and also on Earth; Hugenholtz et al., 2015; Montgomery et al., 2012; Figure 5). Preserved megaripple crests shown in this work (SRs) could represent a main target for the ExoMars rover and inferences made in this work on PBR formative paleoflows can be directly tested. Wheel scuffs of the preserved megaripples crestlines can expose foreset beds dipping in the direction of transport. Microscopic imaging by the Close-UP Imager used in combination with the Mars Multispectral Imager for Subsurface Studies and the spectrometers MicrOmega and Raman Laser can provide detailed grain sizing and compositional data, hinting on past wind conditions and source rocks (Bibring et al., 2017; De Sanctis et al., 2017; Josset et al., 2017; Veneranda et al., 2020). PBRs formative winds can be investigated even if landing will be far from double-crested ridge structures, by looking for aeolian grooves over a specific ridge slope (Hugenholtz et al., 2015). In addition, being eroded into the bright clay-rich unit (Carter et al., 2016; Quantin-Nataf et al., 2021), PBRs provide an easily accessible window into the first 1–2 m of this astrobiologically promising rock unit.

Furthermore, the lander instruments will provide a better assessment on the present-day aeolian environment at the surface (Martín-Torres et al., 2020; Mongelluzzo et al., 2019; Rodionov et al., 2017; Soria-Salinas et al., 2020). The presence of PBRs represents a roughness element that should be taken into account when deriving key parameters for the characterization of the present-day aeolian environment such as

aerodynamic roughness length and wind threshold velocity (Hébrard et al., 2012; Kok et al., 2012; Sullivan et al., 2000; Zimbelman et al., 2015).

4. Conclusions

This work provides the first detailed analysis of a set of ~EW trending ridges interpreted as PBRs, representing erosional footprints left by the passage of megaripples at the surface. The PBR orientation differs from younger TARs/miniTARs suggesting that the wind regime changed from mostly dominant N winds to dominant SE winds. Stratigraphic relationships indicate that the erosion of PBRs occurred after the emplacement of a dark volcanic unit in the Early Amazonian and halted before the emplacement of pristine-looking impacts.

These results indicate that the landing site experienced a complex geological history marked by several episodes of erosion and deposition triggered by the wind action in the Amazonian epoch. By visiting PBRs for the first time, the ExoMars 2022 mission will provide further constraints on PBR formation, shedding light on a past Amazonian environment.

Data Availability Statement

Data are also available at the HiRISE website (http://hirise.lpl.arizona.edu/) or the Planetary Data System (http://pds.nasa.gov/).

Acknowledgments and Samples
S. Silvestro has been partially supported by NASA MDAP Grant 80NSS-C18K1415 and acknowledge L. K. Fenton for her comments. F. Salese is supported by "MarsFirstWater," funded by the European Research Council, Consolidator Grant no. 818602 (P. I. Alberto G. Fairén). D. Vaz acknowledge support from CITEUC (project UID/Multi/00611/2020). M. Pajola has been supported for this study by the Italian Space Agency (ASI-INAF agreement no. 2017-03-17). Supporting information is available in the online version of the paper, including supplemental figures and links to the data used for this investigation (Table S1).

References

Arvidson, R. E., Ashley, J. W., Iii, J. F. B., Chojnacki, M., Cohen, J., Economou, T. E., et al. (2011). Opportunity Mars Rover mission: Overview and selected results from Purgatory ripple to traverses to Endeavour crater. *Journal of Geophysical Research Planets*, *116*(E7), 1–33. https://doi.org/10.1029/2010JE003746

Balme, M., Berman, D. C., Bourke, M. C., & Zimbelman, J. R. (2008). Transverse Aeolian Ridges (TARs) on Mars. *Geomorphology*, *101*(4), 703–720. https://doi.org/10.1016/j.geomorph.2008.03.011

Balme, M., Robson, E., Barnes, R., Butcher, F., Fawdon, P., Huber, B., et al. (2017). Surface-based 3D measurements of small aeolian bedforms on Mars and implications for estimating ExoMars rover traversability hazards. *Planetary and Space Science*, *101*(April), 1–15. https://doi.org/10.1016/j.pss.2017.12.008

Berman, D. C., Balme, M. R., Michalski, J. R., Clark, S. C., & Joseph, E. C. S. (2018). High-resolution investigations of Transverse Aeolian Ridges on Mars. *Icarus*, *312*(September), 247–266. https://doi.org/10.1016/j.icarus.2018.05.003

Beyer, R. A., Alexandrov, O., & McMichael, S. (2018). The Ames Stereo Pipeline: NASA's open source software for deriving and processing terrain data. *Earth and Space Science*, *5*(9), 537–548. https://doi.org/10.1029/2018EA000409

Bhardwaj, A., Sam, L., Martin-torres, F. J., & Zorzano, M. (2019). Distribution and morphologies of Transverse Aeolian Ridges in ExoMars 2020 rover landing site. *Remote Sensing*, *11*(8), 1–17. https://doi.org/10.3390/rs11080912

Bibring, J. P., Hamm, V., Pilorget, C., & Vago, J. L. (2017). The MicrOmega investigation onboard ExoMars. *Astrobiology*, *17*(6–7), 621–626. https://doi.org/10.1089/ast.2016.1642

Bridges, N. T., Bourke, M. C., Geissler, P. E., Banks, M. E., Colon, C., Diniega, S., et al. (2012). Planet-wide sand motion on Mars. *Geology*, *40*(1), 31–34. https://doi.org/10.1130/G32373.1

Carter, J., Quantin, C., Thollot, P., Loizeau, D., Ody, A., & Lozach, L. (2016). Oxia Planum, a clay-laden landing site proposed for the Exomars rover mission: Aqueous mineralogy and alteration scenarios. *47th lunar and planetary science conference*, The Woodlands, Texas, p. 2064. Retrieved from https://www.hou.usra.edu/meetings/lpsc2016/pdf/2064.pdf

Day, M., Anderson, W., Kocurek, G., & Mohrig, D. (2016). Carving intracrater layered deposits with wind on Mars. *Geophysical Research Letters*, *43*(6), 1–7. https://doi.org/10.1002/2016GL068011

Day, M., & Dorn, T. (2019). Wind in Jezero Crater, Mars. *Geophysical Research Letters*, *46*(6), 3099–3107. https://doi.org/10.1029/2019GL082218

De Sanctis, M. C., Altieri, F., Ammannito, E., Biondi, D., De Angelis, S., Meini, M., et al. (2017). Ma-MISS on ExoMars: Mineralogical characterization of the Martian subsurface. *Astrobiology*, *17*(6–7), 612–620. https://doi.org/10.1089/ast.2016.1541

Dickinson, J. L., Kerber, L. A., Fasset, C. I., & Ehlmann, B. L. (2018). A global, blended CTX mosaic of Mars with vectorized seam mapping: A new mosaicking pipeline using principles of non-destructive image editing. 49th lunar and planetary science conference. 49 (pp. 1–2).

Fenton, L. K., Carson, H. C., & Michaels, T. I. (2018). Climate Forcing of Ripple Migration and Crest Alignment in the Last 400 kyr in Meridiani Planum, Mars. *Journal of Geophysical Research: Planets*, *123*(4), 1–15. https://doi.org/10.1002/2017JE005503

Fenton, L. K., Ewing, R. C., Bridges, N. T., & Lorenz, R. (2013). Extraterrestrial aeolian landscapes. Treatise on geomorphology. 11 (pp. 287–312).

Fenton, L. K., Michaels, T. I., & Chojnacki, M. (2015). Late Amazonian aeolian features, gradation, wind regimes, and Sediment State in the Vicinity of the Mars exploration rover opportunity, Meridiani Planum, Mars. *Aeolian Research*, *16*(March), 75–99. https://doi.org/10.1016/j.aeolia.2014.11.004

Foroutan, M., Steinmetz, G., Zimbelman, J. R., & Duguay, C. R. (2018). Megaripples at Wau-an-Namus, Libya: A new analog for similar features on Mars. *Icarus*, *319*(February), 840–851. https://doi.org/10.1016/j.icarus.2018.10.021

Foroutan, M., & Zimbelman, J. R. (2016). Mega-Ripples in Iran: A new analog for transverse aeolian ridges on Mars. *Icarus*, *274*(August), 99–105. https://doi.org/10.1016/j.icarus.2016.03.025

Geissler, P. E. (2014). The birth and death of Transverse Aeolian Ridges on Mars. *Journal of Geophysical Research: Planets*, *119*(12), 2583–2599. https://doi.org/10.1002/2014JE004633

Golombek, M., Robinson, K., Mcewen, A., Bridges, N., Ivanov, B., Tornabene, L., & Sullivan, R. (2010). Constraints on ripple migration at Meridiani Planum from Opportunity and HiRISE observations of fresh craters. *Journal of Geophysical Research Planets*, *115*(E7), 1–34. https://doi.org/10.1029/2010JE003628

Goudie, A. S. (2007). Mega-Yardangs: A global analysis. *Geography Compass*, *1*(1), 65–81. https://doi.org/10.1111/j.1749-8198.2006.00003.x

Grotzinger, J. P., Arvidson, R. E., Iii, J. F. B., Calvin, W., Clark, B. C., Fike, D. A., et al. (2005). Stratigraphy and sedimentology of a dry to wet eolian depositional system, Burns formation, Meridiani Planum, Mars. *Earth and Planetary Science Letters*, *240*(1), 11–72. https://doi.org/10.1016/j.epsl.2005.09.039

Hébrard, E., Listowski, C., Coll, P., Marticorena, B., Bergametti, G., M̈ättänen, A., et al. (2012). An aerodynamic roughness length map derived from extended Martian rock abundance data. *Journal of Geophysical Research*, *117*(4), 1–26. https://doi.org/10.1029/2011JE003942

Hugenholtz, C. H., Barchyn, T. E., & Boulding, A. (2017). Morphology of transverse aeolian ridges (TARs) on Mars from a large sample: Further evidence of a megaripple origin?. *Icarus*, *286*(April), 193–201. https://doi.org/10.1016/j.icarus.2016.10.015

Hugenholtz, C. H., Barchyn, T. E., & Favaro, E. A. (2015). Formation of periodic bedrock ridges on Earth. *Aeolian Research*, *18*(September), 135–144. https://doi.org/10.1016/j.aeolia.2015.07.002

Ivanov, M. A., Slyuta, E. N., Grishakina, E. A., & Dmitrovskii, A. A. (2020). Geomorphological analysis of ExoMars candidate landing site Oxia Planum. *Solar System Research*, *54*(1), 1–14. https://doi.org/10.1134/S0038094620010050

Josset, J. L., Westall, F., Hofmann, B. A., Spray, J., Cockell, C., Kempe, S., et al. (2017). The Close-Up Imager Onboard the ESA ExoMars Rover: Objectives, description, operations, and science validation activities. *Astrobiology*, *17*(6–7), 595–611. https://doi.org/10.1089/ast.2016.1546

Kocurek, G. A., & Ewing, R. C. (2005). Aeolian dune field self-organization – implications for the formation of simple versus complex dune-field patterns. *Geomorphology*, *72*(1–4), 94–105. https://doi.org/10.1016/j.geomorph.2005.05.005

Kok, J. F., Parteli, E. J. R., Michaels, T. I., & Karam, D. B. (2012). The physics of wind-blown sand and dust. *Reports on Progress in Physics*, *75*(10), 1–72. https://doi.org/10.1088/0034-4885/75/10/106901

Laity, J. E. (2009). Landforms, Landscapes, and Processes of Aeolian Erosion. In A. J. Parsons, & A. D. Abrahams (Eds.), *Geomorphology of desert environments* (pp. 1–831) Dordrecht: Springer https://doi.org/10.1007/978-1-4020-5719-9

Lakdawalla, E. (2019). Similarities and differences in the landing sites of ESA's and NASA's 2020 Mars rovers. *Nature Astronomy*, *3*(3), 190–192. https://doi.org/10.1038/s41550-019-0727-x

Malin, M. C., Bell, J. F., Cantor, B. A., Caplinger, M. A., Calvin, W. M., Clancy, R. T., et al. (2007). Context Camera Investigation on board the Mars Reconnaissance Orbiter. *Journal of Geophysical Research*, *112*(5), 1–25. https://doi.org/10.1029/2006JE002808

Martín-Torres, J., Zorzano, M. P., Soria-Salinas, Á., Nazarious, M. I., Konatham, S., Mathanlal, T., et al. (2020). The HABIT (HabitAbility: Brine Irradiation and Temperature) environmental instrument for the ExoMars 2022 Surface Platform. *Planetary and Space Science*, *190*, 104968. https://doi.org/10.1016/j.pss.2020.104968

McEwen, A. S., Eliason, E. M., Bergstrom, J. W., Bridges, N. T., Hansen, C. J., Delamere, W. A., et al. (2007). Mars Reconnaissance Orbiter's High Resolution Imaging Science Experiment (HiRISE). *Journal of Geophysical Research*, *112*, 1–40. E05S02. https://doi.org/10.1029/2005JE002605

McKee, E. D. (1979). A study of global sand seas. In E. D. McKee (Ed.), *USGS professional paper n. 1052* Retrieved from http://pubs.er.usgs.gov/publication/pp1052

Milliken, R. E., Ewing, R. C., Fischer, W. W., & Hurowitz, J. (2014). Wind-blown sandstones cemented by sulfate and clay minerals in Gale Crater, Mars. *Geophysical Research Letters*, *41*(4), 1149–1154. https://doi.org/10.1002/2013GL059097

Mongelluzzo, G., Esposito, F., Cozzolino, F., Molfese, C., Silvestro, S., Franzese, G., et al. (2019). CFD analysis and optimization of the sensor "MicroMED" for the ExoMars 2020 mission. *Measurement*, *147*, 106824. https://doi.org/10.1016/j.measurement.2019.07.052

Montgomery, D. R., Bandfield, J. L., & Becker, S. K. (2012). Periodic bedrock ridges on Mars. *Journal of Geophysical Research*, *117*, E03005. https://doi.org/10.1029/2011JE003970

Pajola, M., Rossato, S., Baratti, E., Pozzobon, R., Quantin, C., Carter, J., & Thollot, P. (2017). Boulder abundances and size-frequency distributions on Oxia Planum-Mars: Scientific implications for the 2020 ESA ExoMars rover. *Icarus*, *296*(November), 73–90. https://doi.org/10.1016/j.icarus.2017.05.011

Quantin-Nataf, C., Carter, J., Mandon, L., Balme, M., Fawdon, P., Davis, J., et al. (2019). ExoMars at Oxia Planum, probing the aqueous-related Noachian environments. *Ninth International Conference on Mars 2019*, *2089*.

Quantin-Nataf, C., Carter, J., Mandon, L., Thollot, P., Balme, M., Volat, M., et al. (2021). Oxia Planum – the landing site for the ExoMars "Rosalind Franklin" Rover Mission: Geological context and pre-landing interpretation (in press). *Astrobiology*, *21*(3), 1–22. https://doi.org/10.1089/ast.2019.2191

Quantin-Nataf, C., Carter, J., Thollot, P., Broyer, J., Lozach, L., Davis, J., et al. (2016). Oxia Planum, the landing site for Exomars 2018. *47th lunar and planetary science conference* pp. 2863. Retrieved from https://www.hou.usra.edu/meetings/lpsc2016/pdf/2863.pdf

Rodionov, D., Korablev, O., Zelenyi, L. M., Vago, J., Bessonov, R., Lipatov, A., et al. (2017). Mars atmospheric measurements planned at ExoMars 2020 Surface Platform. *Sixth International Workshop on the Mars Atmosphere: Modelling and Observations*, 3–5.

Silvestro, S., Vaz, D. A., Di Achille, G., Popa, I. C., & Esposito, F. (2015). Evidence for different episodes of aeolian construction and a new type of wind streak in the 2016 ExoMars landing ellipse in Meridiani Planum, Mars. *Journal of Geophysical Research: Planets*, *120*(4), 760–774. https://doi.org/10.1002/2014JE004756

Soria-Salinas, Á., Zorzano, M. P., Mantas-Nakhai, R., & Martín-Torres, J. (2020). Development of a wind retrieval method for low-speed low-pressure flows for ExoMars. *Applied Thermal Engineering*, *180*, 115752(November), 1–17. https://doi.org/10.1016/j.applthermaleng.2020.115752

Sullivan, R., Banfield, D., Iii, J. F. B., Calvin, W., Fike, D., Golombek, M., et al. (2005). Aeolian processes at the Mars Exploration Rover Meridiani Planum landing site. *Nature*, *436*(July), 58–61. https://doi.org/10.1038/nature03641

Sullivan, R., Greeley, R., Kraft, M., Wilson, G., Golombek, M., Herkenhoff, K., et al. (2000). Results of the Imager for Mars Pathfinder windsock experiment. *Journal of Geophysical Research*, *105*(E10), 24547–24562. https://doi.org/10.1029/1999JE001234

Vago, J. L., Westall, F., Coates, A. J., Jaumann, R., Korablev, O., Ciarletti, V., et al. (2017). Habitability on Early Mars and the Search for Biosignatures with the ExoMars Rover. *Astrobiology*, *17*(6–7), 471–510. https://doi.org/10.1089/ast.2016.1533

Vago, J., Witasse, O., Svedhem, H., Baglioni, P., Haldemann, A., Gianfiglio, G., et al. (2015). ESA ExoMars program: The next step in exploring Mars. *Solar System Research*, *49*(7), 518–528. https://doi.org/10.1134/S0038094615070199

Veneranda, M., Lopez-Reyes, G., Manrique-Martinez, J. A., Sanz-Arranz, A., Lalla, E., Konstantinidis, M., et al. (2020). ExoMars Raman Laser Spectrometer (RLS): Development of chemometric tools to classify ultramafic igneous rocks on Mars. *Scientific Reports*, *10*(1), 1–14. https://doi.org/10.1038/s41598-020-73846-y

Wang, J., Xiao, L., Reiss, D., Hiesinger, H., Huang, J., Xu, Y., et al. (2018). Geological Features and Evolution of Yardangs in the Qaidam Basin, Tibetan Plateau (NW China): A Terrestrial Analogue for Mars. *Journal of Geophysical Research: Planets*, *123*(9), 2336–2364. https://doi.org/10.1029/2018JE005719

Werner, B. T., & Kocurek, G. (1999). Bedform spacing from defect dynamics. *Geology*, *27*(8), 727–730. https://doi.org/10.1130/0091-7613(1999)027<0727

Zimbelman, J. R. (2010). Transverse Aeolian Ridges on Mars: First results from HiRISE images. *Geomorphology*, *121*(1–2), 22–29. https://doi.org/10.1016/j.geomorph.2009.05.012

Zimbelman, J. R., Scheidt, S. P., de Silva, S. L., Bridges, N. T., Spagnuolo, M. G., & Neely, E. M. (2015). Aerodynamic roughness height for gravel-mantled megaripples, with implications for wind profiles near TARs on Mars. *Icarus*, *266*(March), 306–314. https://doi.org/10.1016/j.icarus.2015.11.008